Journal of Quantitative Spectroscopy & Radiative Transfer 330 (2025) 109257

Contents lists available at ScienceDirect

Journal of Quantitative Spectroscopy and Radiative Transfer

journal homepage: www.elsevier.com/locate/jqsrt

The electronic spectra of trifluoroacetic acid and chlorodifluoroacetic acid in the 4.5 – 10.8 eV photon energy region

P.S. Puppi [a], A. Souza Barbosa [a,*], N.C. Jones [b], S.V. Hoffmann [b], U.S. Akther [c], N.J. Mason [d,*], P. Limão-Vieira [a,c,*]

[a] Departamento de Física, Universidade Federal do Paraná, Caixa Postal 19044, 81531-980, Curitiba, Paraná, Brazil
[b] ISA, Department of Physics and Astronomy, Aarhus University, Ny Munkegade 120, DK-8000, Aarhus C, Denmark
[c] Atomic and Molecular Collisions Laboratory, CEFITEC, Department of Physics, NOVA School of Science and Technology, Universidade NOVA de Lisboa, 2829-516, Caparica, Portugal
[d] Centre for Astrophysics and Planetary Science, School of Physics and Astronomy, University of Kent, Canterbury, United Kingdom

ARTICLE INFO

Keywords:
Trifluoroacetic acid
Chlorodifluoroacetic acid
Photoabsorption
Cross-section
Rydberg states

ABSTRACT

Synchrotron radiation has been used to record for the first time absolute vacuum ultraviolet photoabsorption cross-sections of trifluoroacetic acid (TFA) and chlorodifluoroacetic acid (CDFA) in the 4.5–10.8 eV energy range. In order to further our knowledge of the major electronic transitions and thus help interpret the photoabsorption data, theoretical calculations using time-dependent density functional theory (TD-DFT) level have been performed. These calculations have provided important information on the nature of the excited electronic states which have been assigned to valence, mixed valence-Rydberg and Rydberg transitions. Due to the lack of any information about CDFA ionic states, we also provide Equation-of-Motion Coupled-Cluster Single and Doubles (EOM-CCSD) vertical ionisation energies. Photolysis lifetimes in the Earth's atmosphere for both chemical compounds have also been estimated from the absolute photoabsorption cross-section data.

1. Introduction

Trifluoroacetic acid (TFA), $CF_3C(O)OH$, and chlorodifluoroacetic acid (CDFA), $CF_2ClC(O)OH$, are two halogenated-derivatives of acetic acid, $CH_3C(O)OH$. We have previously investigated acetic acid, given its role in the metabolic processes of several forms of life and for occurring naturally from the action of certain bacteria in foods or liquids containing sugars or ethanol [1].

TFA is a product of the atmospheric oxidation of several hydrofluorocarbons, e.g. HCFC-123 (CF_3CHCl_2), HCFC-124 (CF_3CHFCl), and HFC-134a (CF_3CH_2F), used as coolants in air conditioning and refrigeration processes as replacements for ozone-depleting substances [2–7]. Additionally, the inhalation process of anaesthetic halothane [8,9] has been reported as a major precursor of TFA formation [4]. In the terrestrial atmosphere, due to its high solubility, TFA may be removed through rainout or by surface/ocean deposition [3,5,10]. However, neither photolysis nor reactions with $^{\bullet}OH$ radicals have been assessed as a relevant sink mechanism in the troposphere, while recent studies have noted that atmospheric TFA may also contribute to the formation of aerosols which may be relevant in climate change [11].

CDFA is a degradation product of chlorofluorocarbons such as CFC-113 ($C_2Cl_3F_3$) and to a lesser extent of hydrofluorocarbon HCFC-142b ($C_2H_3ClF_2$) [6,7]. It has been detected in rain and snow fall in different regions across Canada, where low concentrations of CDFA (as well as TFA) are reported, however both chemical compounds present a low ecotoxicological risk [6]. Despite recent efforts within the international scientific community to determine the impact of these molecules in the Earth's atmosphere, the lack of a comprehensive and accurate assessment of their electronic state spectroscopy has hindered these studies and therefore provides a motivation for this work.

A thorough literature survey of the lowest-lying neutral and ionic states, shows that TFA has only been investigated by a few spectroscopic experimental methods. These include experimental data on the valence shell He(I) and He(II) [12–14], and threshold [15] photoelectron spectroscopies, studies on the absorption [16–19], photodissociation dynamics [20–24] and infrared and Raman spectroscopies [25–28]. Additionally, TFA has also been investigated by theoretical methods for absorption [18] and photodissociation [29]. Regarding CDFA we are only aware of a single work on the structure and geometrical parameters [30].

* Corresponding authors.
E-mail addresses: alessandra@fisica.ufpr.br (A.S. Barbosa), N.J.Mason@kent.ac.uk (N.J. Mason), plimaovieira@fct.unl.pt (P. Limão-Vieira).

https://doi.org/10.1016/j.jqsrt.2024.109257
Received 25 August 2024; Accepted 30 October 2024
Available online 1 November 2024

In this joint experimental and theoretical study, we present a novel and comprehensive study of TFA and CDFA electronic state spectroscopy, over a wide photon energy range from 4.5 eV up to 10.8 eV High-resolution vacuum ultraviolet photoabsorption spectra were obtained with a synchrotron radiation light source, and time-dependent density functional theory (TD-DFT) calculations for the lowest-lying neutral and ionic states have been used to help assign the major electronic transitions.

Section 2 of this paper gives a summary of the structure and properties of trifluoroacetic acid and chlorodifluoroacetic acid, while Section 3 provides a short description of the experimental setup, and the computational details used in the calculations. Section 4 is devoted to the results and discussion of the valence, mixed valence-Rydberg and Rydberg excitations of both compounds, and the absolute photoabsorption cross-sections used to estimate photolysis rates from 0 to 50 km altitude in the Earth's atmosphere. The main conclusions that can be drawn from this study are given in Section 5, and additional details can be found in the Supplementary Material (SM).

2. Structure and properties of trifluoroacetic acid and chlorodifluoroacetic acid

The calculated outermost valence electronic configuration of trifluoroacetic acid (TFA) in the $\tilde{X}^1A'$ state is: … $(5a'')^2$ $(17a')^2$ $(18a')^2$ $(6a'')^2$ $(7a'')^2$ $(19a')^2$ $(8a'')^2$ $(20a')^2$ (see Fig. S1). The most active molecular orbitals relevant for the photoabsorption transitions from which promotion of electrons have been assigned, are the (HOMO), 20a′, and the (HOMO-1), 8a″, with O 2p lone pair orbital ($\overline{n}_O$) and n_O/π characters. Other molecular orbitals have also been assigned to (HOMO-2), 19a′, and (HOMO-4), 6a″, with $\overline{n}_F/\sigma_{CC/CO}$ and n_F/π character. The photoabsorption features in Figs. 1a, 2a and 3a, are assigned in Table 1a to valence, mixed valence-Rydberg and Rydberg electronic excitations, while Tables S1–S3 list the complete set of calculated transition energies and oscillator strengths at the TD-DFT level of theory with different functionals. The TFA photoabsorption spectrum displays features assigned to vibronic transitions, with the main fundamental vibrational modes available from the infrared absorption data [27,28] and the calculated frequencies (B3LYP/aug-cc-pVQZ) of the neutral and cation ground states (Table S4).

Chlorodifluoroacetic acid ($CF_2ClCOOH$) has two conformers at room temperature with conformer #1 (doubly degenerated) showing the Cl atom pointing out of the C = O plane, while in conformer #2 the Cl atom is rotated to the C–C=O plane (Fig. S2). According to our B3LYP/aug-cc-pVQZ calculations, the dihedral angle between the Cl atom and the C–C=O plane is 99.8° The population analysis yields 94.7 % for conformer #1 and 5.3 % for conformer #2, the former being more stable than the latter by 0.0563 eV The ground-state electronic configurations of conformer #1 and conformer #2 have C_1 (A) and C_S (A′ and A″) symmetries, with calculated outermost valence electronic configurations of : … $(24a)^2$ $(25a)^2$ $(26a)^2$ $(27a)^2$ $(28a)^2$ $(29a)^2$ $(30a)^2$ $(31a)^2$ $(32a)^2$ and $(19a')^2$ $(6a'')^2$ $(7a'')^2$ $(20a')^2$ $(21a')^2$ $(8a'')^2$ $(9a'')^2$ $(22a')^2$ $(23a')^2$. A close inspection of the ground-state MOs' character (see Fig. S4) shows that, for conformer #1 the highest occupied molecular orbital (HOMO), 32a, and the (HOMO-1), 31a, are mainly $\overline{n}_O$ /$\overline{n}_{Cl}$ and n_{Cl}. The third highest occupied molecular orbital (HOMO-2), 30a, is the Cl 3p lone pair orbital ($\overline{n}_{Cl}$) and the (HOMO-3), 29a, is of n_{Cl}/π character. For conformer #2, the (HOMO), 23a′, and the (HOMO-1), 22a′, are mainly $\overline{n}_O/\overline{n}_{Cl}$ and $\overline{n}_{Cl}$. The (HOMO-2), 9a″, is n_{Cl}/n_F and the (HOMO-3), 8a″, is of n_O character. The photoabsorption spectrum (Figs. 1b, 2b and 3b) shows bands that have been assigned to electronic excitations, due to promotion of an electron from those MOs to valence, mixed valence-Rydberg and Rydberg character orbitals (see Table 1b for the calculated dominant excitation energies and oscillator strengths). Note that in Tables S5–S10 we list the complete set of calculated transition energies and oscillator strengths at TD-DFT level of theory with different functionals.

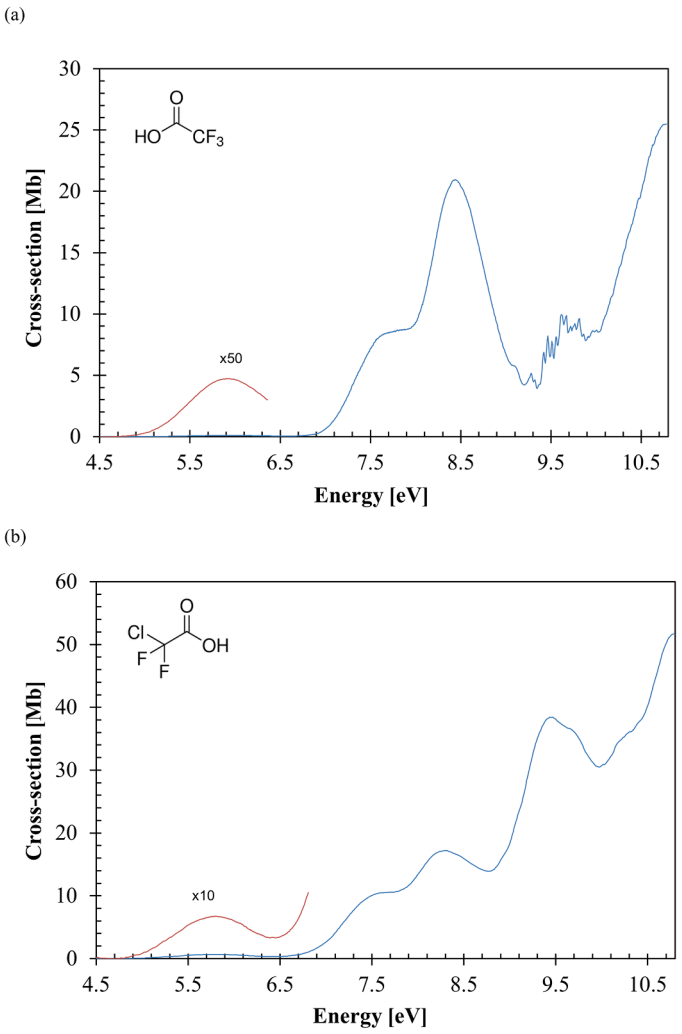

Fig. 1. The VUV photoabsorption cross-section in the 4.5–10.8 eV range for: (a) trifluoroacetic acid; (b) chlorodifluoroacetic acid. Inset shows the structure of the molecules.

The fine structure that is noticeable in the photoabsorption spectrum of trifluoroacetic acid (Figs. 2a and 3a) has been assigned from the available energies (and wavenumbers) in the ground electronic state to 0.048 eV (390 cm^{-1}) for CF_3 rocking, $\nu'_{15}(a')$ mode [28], and denoted X^n_m, with m and n indicating the initial and final vibrational states for the assignments of the vibronic structure (X). The photoabsorption spectrum of chlorodifluoroacetic acid (Figs. 2b and 3b) does not show any discernible features reminiscent of vibronic excitations, so no attempt has been made to propose any.

The lowest experimental adiabatic/vertical ionisation energies, needed to calculate the quantum defects associated with transitions to Rydberg orbitals, are for TFA taken from the work of Sweigart and Turner [14] and Carnovale et al. [13] to be 11.46 eV $(20a')^{-1}$ and 13.16 eV $(8a'')^{-1}$, whereas for CDFA conformer #1/conformer #2 they are taken from the present calculations in Table S11 to be 11.60 eV $(32a)^{-1}$/11.72 eV $(23a')^{-1}$ and 12.58 eV $(31a)^{-1}$/12.55 eV $(22a')^{-1}$, respectively.

3. Experimental and theoretical methods

High-resolution VUV photoabsorption spectra of trifluoroacetic acid and chlorodifluoroacetic acid (Figs. 1a and 1b) were recorded at the UV1 beam line using synchrotron radiation produced by the ASTRID storage

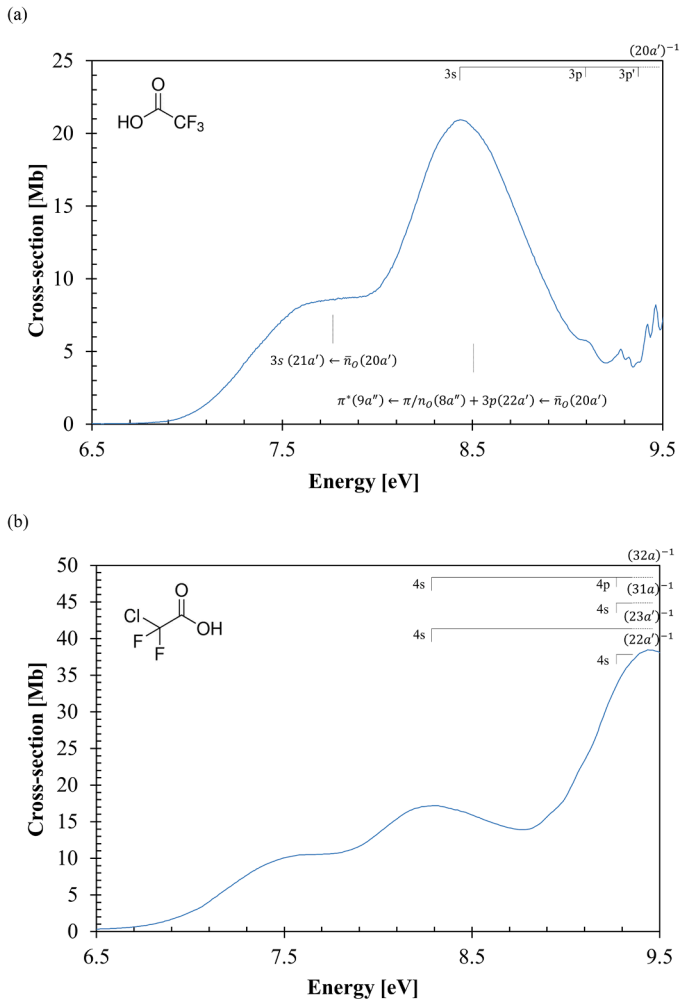

Fig. 2. The VUV photoabsorption cross-section for: (a) trifluoroacetic acid in the 6.5–9.5 eV range; (b) chlorodifluoroacetic acid in the 6.5–9.5 eV range.

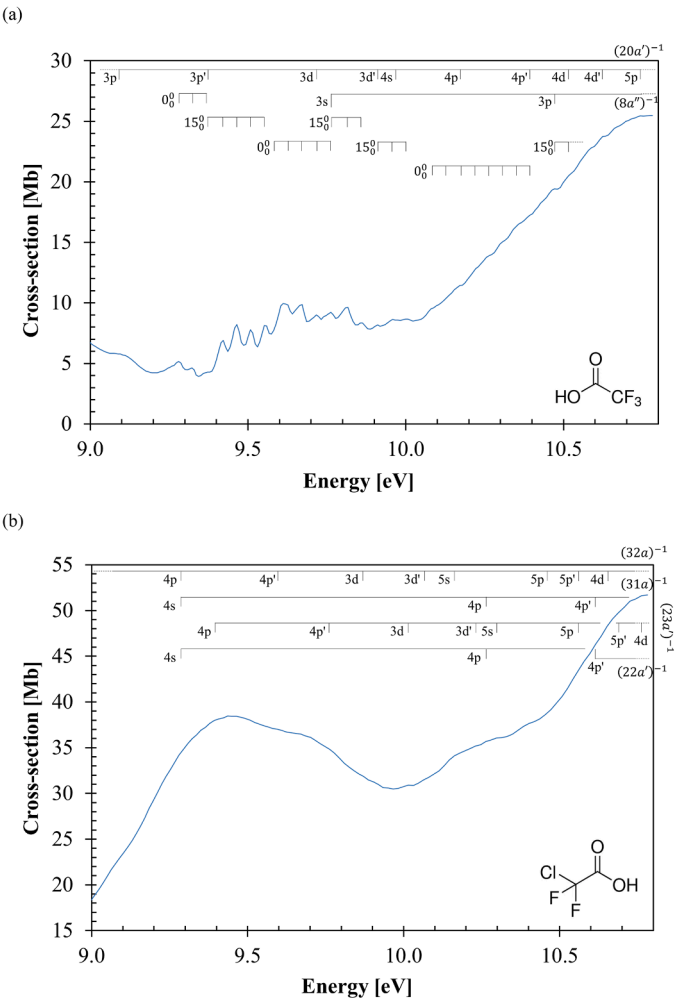

Fig. 3. The VUV photoabsorption cross-section in the 9.0–10.8 eV range for: (a) trifluoroacetic acid; (b) chlorodifluoroacetic acid. See text for details.

ring, Aarhus University, Denmark. The experimental set up has been systematically described on other occasions before [31], and so only a short description is given here. Briefly, monochromatized light with a resolution of better than 0.08 nm passes through an absorption static gas cell that is filled with vapour of the molecular compound under investigation. The transmission windows (MgF_2) used to enclose the absorption cell set the lower wavelength limit of detection (115 nm), and the transmitted UV light is detected by a photomultiplier tube (PMT). A capacitance manometer (Baratron) was used to monitor the sample's absolute pressure in the absorption gas cell. To avoid any saturation effects in the data recorded, absorption cross-sections were carefully measured using a pressure within the range 0.12–1.32 mbar which has attenuations of 60 % or less. Absolute photoabsorption cross-section values, σ, in units of megabarn (1Mb $\equiv 10^{-18}$ cm^2), were obtained using the Beer-Lambert attenuation law: $I_t = I_0 e^{(-N\sigma l)}$, where I_t is the radiation intensity transmitted through the gas sample, I_o is that through the evacuated cell, N the molecular number density, and l the absorption path length (15.5 cm).

The synchrotron beam ring current was monitored throughout the collection of each spectrum, and background scans were recorded with the cell evacuated. Accurate cross-section values are obtained by recording the VUV spectrum in small (5 or 10 nm) sections, allowing an overlap of at least 10 points between the adjoining sections. The accuracy of the photoabsorption cross-section is estimated to within ± 5 %, although for low values of the absorption ($I_o \approx I_t$) the uncertainty increases as a percentage of the measured cross-section. The proposed assignments of the recorded absorption features are listed in Tables 2a and 2b and Tables 3a and 3b.

The liquid samples of trifluoroacetic acid (TFA, CAS number: 76–05–1) and chlorodifluoroacetic acid (CDFA, CAS number: 76–04–0) used in the VUV photoabsorption measurements were purchased from Sigma-Aldrich, with a stated purity of ≥ 99 % and 98 %. The samples were degassed through repeated freeze-pump-thaw cycles prior to input into the gas cell.

The theoretical methodology employed has been discussed in detail in previous publications (see e.g. [32,33]) and so, once again, only a brief description is given here. The optimised geometries of TFA and CDFA (Figs. S1 and S2) were obtained with DFT calculations, with the B3LYP functional and Dunning's augmented correlation consistent valence quadruple-ζ (aug-cc-pVQZ) basis set, as implemented in the package GAMESS-US [34]. The ground state geometry and harmonic vibrational frequencies of the neutral singlet state (S_0) and ionic doublet state (D_0^+) of TFA (Table S4) were obtained with use of GAMESS-US [35] at the same level of theory.

The vertical excitation energies and oscillator strengths of TFA and CDFA were obtained for the ground-state optimised molecular geometries of both molecules, employing TD-DFT [36,37] with the same functional and basis set employed in the geometries optimisation. In Tables 1a and 1b, we show only the dominant vertical excitation energies, whereas a complete description of all computed singlet excited states for TFA and CDFA are shown in Tables S1 and S5-S6, respectively.

Table 1a
Calculated dominant vertical excitation energies (TD-DFT/B3LYP/aug-cc-pVQZ) and oscillator strengths of trifluoroacetic acid compared where possible with corresponding experimental data and other work in the literature (energies in eV). See text for details.

Trifluoroacetic acid				$E_{exp.}$ (eV)[a]	Cross-section (Mb)	E (eV) [16]
State	E (eV)	f_L	Dominant excitations			
$\tilde{X}\ ^1A'$						
$1\ ^1A''$	5.600	0.00057	$\pi^*(9a'')\leftarrow\bar{n}_O(20a')$ (99 %)	5.904	0.10	0.07
$2\ ^1A'$	7.351	0.03236	$3s\ (21a')\leftarrow\bar{n}_O(20a')$ (91 %)	7.69(6)	8.49	8.22
$3\ ^1A'$	8.289	0.13864	$\pi^*(9a'')\leftarrow\pi/n_O(8a'')$ (73 %) + $3p(22a')\leftarrow\bar{n}_O(20a')$ (10 %)	8.44(6)	20.95	17.59
$5\ ^1A'$	8.914	0.02972	$3p'(23a')\leftarrow\bar{n}_O(20a')$ (91 %)	9.280	5.17	–
$9\ ^1A'$	9.754	0.02287	$\pi^*(9a'')\leftarrow\pi/n_F(6a'')$ (59 %) + $3d(26a')\leftarrow\bar{n}_O(20a')$ (37 %)	9.611	9.94	10.13
$11\ ^1A'$	9.992	0.05119	$3s\ (21a')\leftarrow\sigma_{CC/CO}/\bar{n}_F(19a')$ (90 %)	9.999	8.67	–
$13\ ^1A'$	10.407	0.03068	$3d'(27a')\leftarrow\bar{n}_O(20a')$ (95 %)	10.772	25.48	–

[a] the last decimal of the energy value is given in brackets for these less-resolved features.

Table 1b
Calculated dominant vertical excitation energies (TD-DFT/B3LYP/aug-cc-pVQZ) and oscillator strengths of chlorodifluoroacetic acid conformers (energies in eV). See text for details.

Chlorodifluoroacetic acid conformer #1				$E_{exp.}$ (eV)[a]	Cross-section (Mb)
State	E (eV)	f_L	Dominant excitations		
$\tilde{X}\ ^1A$					
$2\ ^1A$	5.439	0.00947	$\sigma^*_{CCl}(33a)\leftarrow\bar{n}_{Cl}/\bar{n}_O(32a)$ (92 %)	5.826	0.67
$5\ ^1A$	7.819	0.06351	$\sigma^*_{CCl}(33a)\leftarrow\pi/n_{Cl}(29a)$ (71 %) + $4s(34a)\leftarrow\bar{n}_{Cl}/\bar{n}_O(32a)$ (11 %)	7.597	10.47
$9\ ^1A$	8.336	0.05303	$4p(36a)\leftarrow\bar{n}_{Cl}/\bar{n}_O(32a)$ (49 %) + $4s(34a)\leftarrow\bar{n}_{Cl}(30a)$ (34 %)	8.299	17.19
$15\ ^1A$	8.987	0.04031	$4p(36a)\leftarrow n_{Cl}(31a)$ (85 %)	8.94(6)	16.76
$16\ ^1A$	9.155	0.05235	$4p'(35a)\leftarrow\pi/n_{Cl}(29a)$ (42 %) + $4p(36a)\leftarrow\bar{n}_{Cl}(30a)$ (33 %) + $5s(39a)\leftarrow\bar{n}_{Cl}/\bar{n}_O(32a)$(14 %)	9.436	38.47
$39\ ^1A$	10.224	0.10065	$5s(39a)\leftarrow\bar{n}_{Cl}(31a)$ (32 %) + $3d(40a)\leftarrow\bar{n}_{Cl}(30a)$ (14 %) + $3d(40a)\leftarrow n_{Cl}(31a)$ (15 %)	10.29(8)	36.07
Chlorodifluoroacetic acid conformer #2				$E_{exp.}$ (eV)[a]	Cross-section (Mb)
State	E (eV)	f_L	Dominant excitations		
$\tilde{X}\ ^1A'$					
$1\ ^1A''$	5.548	0.00024	$\sigma^*_{CCl}/\pi^*(10a'')\leftarrow\bar{n}_{Cl}/\bar{n}_O(23a')$ (98 %)	5.826	0.67
$2\ ^1A'$	7.146	0.04757	$4s(24a')\leftarrow\bar{n}_{Cl}/\bar{n}_O(23a')$ (91 %)	7.597	10.47
$6\ ^1A'$	8.267	0.10299	$\sigma^*_{CCl}/\pi^*(10a'')\leftarrow n_O(8a'')$ (38 %) + $4s(24a')\leftarrow\bar{n}_{Cl}(22a')$ (32 %) + $\sigma^*_{CCl}(25a')\leftarrow\bar{n}_{Cl}(22a')$ (22 %)	8.299	17.19
$9\ ^1A'$	8.938	0.06589	$4p(26a')\leftarrow\bar{n}_{Cl}(22a')$ (85 %)	8.94(6)	16.76
$12\ ^1A'$	9.536	0.03388	$\sigma^*_{CCl}/\pi^*(10a'')\leftarrow\bar{n}_F(7a'')$ (30 %) + $4s(24a')\leftarrow\sigma_{CC/CO}(21a')$ (15 %) + $4p'(11a'')\leftarrow n_F/n_{Cl}(9a'')$ (39 %)	9.436	38.47
$19\ ^1A'$	10.044	0.05205	$\sigma^*_{CCl}(25a')\leftarrow\sigma_{CC/CO}(21a')$ (46 %) + $\sigma^*_{CCl}/\pi^*(10a'')\leftarrow\bar{n}_{Cl}(6a'')$ (38 %)	10.29(8)	36.07

[a] the last decimal of the energy value is given in brackets for these less-resolved features.

The calculated vertical ionisation energies (eV) of CDFA at the EOMCCSD/aug-cc-pVTZ level are shown in Table S11.

4. Results and discussion

Absolute cross-section high-resolution VUV photoabsorption spectra of TFA and CDFA, recorded at room temperature in the photon energy range 4.5–10.8 eV, are shown in Fig. 1a and 1b, respectively, while expanded views of the measured cross-sections are shown in Figs. 2 and 3. The major absorption bands can be classified as electronic excitations from valence, mixed valence-Rydberg and from Rydberg series (Section 4.4) converging to the lowest-lying ionic states. Tables 1a and 1b lists the calculated vertical excitation energies and oscillator strengths from TD-DFT B3LYP/aug-cc-pVQZ calculations for TFA and CDFA, compared with the experimental results. We note a very good level of agreement (to within ± 6 %) between the calculated and experimental data. In order to check the level of accuracy between both sets of data, we have tested other functionals and levels of theory with the results given in Tables S2–S3 and Tables S7–S10 for TCA and CDFA molecules. Generally speaking, we do not observe any relevant discrepancies between TD-DFT/CAMB3LYP/aug-cc-pVQZ and TD-DFT/PBE0/aug-cc-pVQZ levels of theory. The TFA spectrum exhibits fine structures above 9.0 eV reminiscent of vibronic transitions, with the most relevant vibrational mode assigned to CF_3 rocking, $\nu'_{15}(a')$ (Table 2), whereas no discernible fine structure and/or vibrational quanta have been assigned in the CDFA spectrum due to the broad and structureless nature of the electronic transitions. The photoabsorption features above 8.2 eV in the spectra of TFA and CDFA, are largely due to the overlap of different Rydberg electronic states. The assignments are depicted in Figs. 2 and 3 and the values listed in Table 3.

Although not shown in Fig. 1 the photoabsorption bands of acetic acid [1] show some resemblance with TFA and CDFA for the overall shapes, however the TFA and CDFA show less fine structure than acetic acid the latter and the bands are slightly blue shifted. Another interesting aspect pertains to the magnitude of the cross-section, where TFA's absorption feature peaking at 8.434 eV is the only peak exhibiting a higher value (20.95 Mb) than the related band in acetic acid at 8.349 eV (16.02 Mb). Most of the CDFA bands, with the exception between 9.9 and 10.6 eV, show higher magnitudes than the analogues in acetic acid. It is also interesting to note that the lowest-lying absorption bands of TFA and CDFA are red-shifted relative to $CH_3C(O)OH$ and their magnitudes increase in the sequence $CF_3C(O)OH < CH_3C(O)OH < CF_2ClC(O)OH$. The major electronic transitions of TFA and CDFA photoabsorption bands are assigned to the promotion of an electron from the (HOMO) and (HOMO-1) to out-of-plane oxygen and chlorine lone pairs (n_O and n_{Cl}) to lowest unoccupied molecular orbitals (Tables 1 and 2, Figs. S3 and S4). We will now discuss the absorption features in the different photon energy ranges in detail making use of the quantum chemical calculations.

Table 2
Proposed vibrational assignments of trifluoroacetic acid absorption bands in the photon energy range 9.0 – 10.8 eV[a]. Energies in eV. See text for details.

assignment	energy	ΔE (υ_{15})
$3p'(23a')\leftarrow\overline{n}_O(20a')$, $(5^1A'\leftarrow\widetilde{X}^1A')$		
0_0^0	9.280	–
15_0^1	9.322	0.042
15_0^2	9.36(4)(b,w)	0.042
$3p'(20a')^{-1}$	9.37(9)(b,w)	–
15_0^1	9.421	0.042
15_0^2	9.464	0.043
15_0^3	9.508	0.044
15_0^4	9.55(2)(b)	0.044
$\pi^*(9a'')\leftarrow\pi/n_F(6a'')+3d(26a')\leftarrow\overline{n}_O(20a')$, $(9^1A'\leftarrow\widetilde{X}^1A')$		
0_0^0	9.58(2)(s)	–
15_0^1	9.61(9)(s)	0.037
15_0^2	9.671	0.052
15_0^3 /$3d(20a')^{-1}$	9.717	0.046
15_0^4 /$3s(8a'')^{-1}$	9.763	0.046
$3s(5a'')^{-1}$	9.763	–
15_0^1	9.81(7)(b)	0.054
15_0^2	9.86(4)(b)	0.047
$3s\ (21a')\leftarrow\sigma_{CC/CO}/\overline{n}_F(19a')$, $(11^1A'\leftarrow\widetilde{X}^1A')$		
$3d'(20a')^{-1}$	9.91(9)(w)	–
15_0^1	9.959	0.040
15_0^2	10.00(7)(b)	0.048
$3d'(27a')\leftarrow\overline{n}_O(20a')$, $(13^1A'\leftarrow\widetilde{X}^1A')$		
0_0^0	10.08(8)(s)	–
15_0^1	10.12(9)(s,w)	0.041
15_0^2 /$4p(20a')^{-1}$	10.17(9)(s)	0.050
15_0^3	10.22(1)(s)	0.042
15_0^4	10.26(4)(s)	0.043
15_0^5	10.30(6)(s)	0.042
15_0^6	10.34(9)(s)	0.043
15_0^7 /$4p'(20a')^{-1}$	10.39(3)(s)	0.044
$3p(8a'')^{-1}$	10.47(2)(s)	–
15_0^1 /$4d(20a')^{-1}$	10.51(6)(b,w)	0.044
	$\overline{\Delta E}$	0.044

[a] (s) shoulder structure; (w) weak feature (the last decimal of the energy value is given in brackets for these less-resolved features);.

4.1. Photon energy region 4.5 – 6.5 eV

4.1.1. Trifluoroacetic acid

This band exhibits a broad and structureless spectral feature (see Fig. 1a), that has been assigned in Table 1a to the $\pi^*(9a'')\leftarrow\overline{n}_O(20a')$, $(1^1A''\leftarrow\widetilde{X}^1A')$ transition with an oscillator strength of ≈ 0.0006. The photoabsorption cross-section peaks at 5.904 eV with a value of 0.1 Mb, which is in reasonable agreement with Basch et al. [16] who states a vertical excitation energy of 5.965 eV and 0.07 Mb, however there is a poor agreement with Rattigan et al.'s [17] data where the band peaks at 5.636 eV (220 nm) with a cross-section value of 0.08 Mb. This rather low intensity absorption feature is due to the A′ electronic ground state transition to the upper excited A″ state, which is polarised normal to the plane of the molecule containing the C–C(O)O group. Such behaviour was previously observed in case of formic acid [38]. Additionally, the 193 nm (6.424 eV) photodissociation dynamics studies of Kwon et al. [20] and SenGupta et al. [23], have shown that bond-breaking yielding OH occurs mainly from the singlet state S_1, with an exit barrier of 14–15 kcal/mol (~0.61–0.65 eV), or via intersystem crossing to lower energy triplet states (T_1 and T_2). Thus, OH abstraction from TFA occurs with a quantum yield of $\varphi_{OH}(CF_3C(O)OH) = 0.4$, while the optically excited S_1 state can undergo radiation-less transition via internal conversion to the ground state (S_0) [20].

At the lowest-lying energy side of the band our calculations predict the contribution of a triplet state at 4.987 eV assigned to the $\overline{n}_O(20a')\rightarrow\pi^*(9a'')$ transition, while at a slightly higher energy of 5.649 eV it may be due to $n_O/\pi(8a'')\rightarrow\pi^*(9a'')$ (Table S12). While such optically forbidden transitions are typically not visible in the experimental photoabsorption spectrum, we are not aware of any electron energy loss spectroscopy measurements to confirm the presence of any of these.

Finally, Basch et al. [16] report the presence of dimer formation from the gas-phase spectra obtained at a pressure value of 57 mm Hg (76 mbar) in a 1-cm absorption cell. The ionisation energies of trifluoroacetic dimers from the photoelectron spectroscopy data of Carnovale and co-workers [13], have been used to obtain the different members of Rydberg series based on the quantum defects. The expected energy positions do not match any evident features, meaning that in the present room temperature spectrum we have no hint of dimers contributing to the absorption spectrum.

4.1.2. Chlorodifluoroacetic acid

The lowest-lying absorption band is both broad and structureless (Fig. 1b), showing a photoabsorption cross-section peaking at 5.826 eV and magnitude of 0.67 Mb, and is ~ 6.7 more intense than the corresponding in TFA. The calculations in Table 1b for conformers #1/#2 assign the electronic transitions to the promotion of an electron from the HOMO (32a/23a′) to the LUMO (33a/10a″) as $\sigma^*_{CCl}(33a)\leftarrow\overline{n}_{Cl}/\overline{n}_O(32a)$, $\left(2^1A\leftarrow\widetilde{X}^1A\right)$ and $\sigma^*_{CCl}/\pi^*(10a'')\leftarrow\overline{n}_{Cl}/\overline{n}_O(23a')$, $\left(1^1A''\leftarrow\widetilde{X}^1A'\right)$, with oscillator strengths of ≈0.0095/0.0002. Following the same rationale for TFA, the calculations in Table S12 predict the presence of triplet states, that certainly need further investigation which is beyond the scope of this contribution. The lowest energy has been calculated at 4.839/4.957 eV for conformers #1/#2 and assigned to the $\overline{n}_{Cl}/\overline{n}_O(32a)\rightarrow\sigma^*_{CCl}(33a)/\overline{n}_{Cl}/\overline{n}_O(23a')\rightarrow\sigma^*_{CCl}/\pi^*(10a'')$ transitions, whereas at 5.578/5.629 eV these are due to $\pi/n_{Cl}(29a)\rightarrow\sigma^*_{CCl}(33a)+\ \overline{n}_{Cl}(31a)\rightarrow\sigma^*_{CCl}(33a)/n_O(8a'')\rightarrow\sigma^*_{CCl}/\pi^*(10a'')$.

4.2. Photon energy region 6.5 – 9.5 eV

4.2.1. Trifluoroacetic acid

The absorption band in the 6.5 – 9.5 eV photon energy range is shown in detail in Fig. 2a with the assignments of the spectral features in Tables 2 and 3a. The absorption in this region is particularly strong, with two main transitions with local maxima cross-sections of 8.49 and 20.95

Table 3a
Energy values (eV), quantum defects (δ) and assignments of the Rydberg series converging to $(20a')^{-1}\ \widetilde{X}^2A'$ and $(8a'')^{-1}\ \widetilde{A}^2A''$ ionic states of trifluoroacetic acid. See text for details.

E_n	δ	Assignment	E_n	δ	Assignment
$(IE_1)_{ad}$ = 11.46 eV $(20a')^{-1}$			**$(IE_2)_v$ = 13.16 eV** $(8a'')^{-1}$		
($ns\leftarrow20a'$)			($ns\leftarrow8a''$)		
8.44(6)(b)	0.88	3s	9.763	1.00	3s
9.96(7)(b,w)	0.98	4s			
($np\leftarrow20a'$)			($np\leftarrow8a''$)		
9.09(0)(s)	0.60	3p	10.47(2)(s)	0.75	3p
10.17(9)(s)	0.74	4p			
10.74(4)(s,w)	0.64	5p			
($np'\leftarrow20a'$)					
9.37(9)(b,w)	0.44	3p'			
10.39(3)(s,w)	0.43	4p'			
($nd\leftarrow20a'$)					
9.717	0.21	3d			
10.51(6)(b,w)	0.20	4d			
($nd'\leftarrow20a'$)					
9.919	0.03	3d'			
10.62(4)(w)	−0.03	4d'			

(b) broad feature; (w) weak structure; (s) shoulder structure (the last decimal on the energy value is given in brackets for these less-resolved features).

Mb assigned to $3s\,(21a')\leftarrow\bar{n}_O(20a')$, $(2^1A'\leftarrow\tilde{X}^1A')$ and $\pi^*(9a'')\leftarrow\pi/n_O(8a'')+3p(22a')\leftarrow\bar{n}_O(20a')$, $(3^1A'\leftarrow\tilde{X}^1A')$. These electronic transitions with vertical values at 7.69(6) eV and at 8.44(6) eV have oscillator strengths of $f_L\approx0.0324$ and $f_L\approx0.1386$ from the TD-DFT calculation in Table 1a. The proposed vibrational assignments are due to CF_3 rocking, $\nu'_{15}(a')$ mode (Table 2), with average values of 0.044 eV These values are lowered from the ground-state of TFA (390 $cm^{-1}\equiv0.048$ eV), suggesting a broadening of the potential energy surfaces involved in such electronic excitations. The structural features observed above 9.2 eV are also broad and originate from the contribution of the valence character mixed with the Rydberg $(20a')^{-1}$ and $(5a'')^{-1}$ series, these discussed in more detail in Section 4.4 (see also Table 3a).

4.2.2. Chlorodifluoroacetic acid

Regarding the electronic excitations of conformers #1/#2 in this energy band (Fig. 2b), features have been assigned to mixed valence-Rydberg and Rydberg characters at 7.597 eV (10.47 Mb) to $4s(34a)\leftarrow\bar{n}_{Cl}/\bar{n}_O(32a)+\sigma^*_{CCl}(33a)\leftarrow\pi/n_{Cl}(29a)$, $(5^1A\leftarrow\tilde{X}^1A)/4s(24a')\leftarrow\bar{n}_{Cl}/\bar{n}_O(23a')$, $(2^1A'\leftarrow\tilde{X}^1A')$, at 8.299 eV (17.19 Mb) to $4p(36a)\leftarrow\bar{n}_{Cl}/\bar{n}_O(32a)+4s(34a)\leftarrow\bar{n}_{Cl}(30a)$, $(9^1A\leftarrow\tilde{X}^1A)/\sigma^*_{CCl}/\pi^*(10a'')\leftarrow n_O(8a'')+4s(24a')\leftarrow\bar{n}_{Cl}(22a')+\sigma^*_{CCl}(25a')\leftarrow\bar{n}_{Cl}(22a')$, $(6^1A'\leftarrow\tilde{X}^1A')$, at 8.94(6) eV (16.76 Mb) to $4p(36a)\leftarrow n_{Cl}(31a)$, $(15^1A\leftarrow\tilde{X}^1A)/4p(26a')\leftarrow\bar{n}_{Cl}\ (22a')$, $(9^1A'\leftarrow\tilde{X}^1A')$ and at 9.436 eV (38.47 Mb) to $4p'(35a)\leftarrow\pi/n_{Cl}(29a)+4p(36a)\leftarrow\bar{n}_{Cl}(30a)+5s(39a)\leftarrow\bar{n}_{Cl}/\bar{n}_O(32a)$, $(16^1A\leftarrow\tilde{X}^1A)/\sigma^*_{CCl}/\pi^*(10a'')\leftarrow\bar{n}_F(7a'')\ +4s(24a')\leftarrow\sigma_{CC/CO}(21a')+4p'(11a'')\leftarrow n_F/n_{Cl}(9a'')$, $(12^1A'\leftarrow\tilde{X}^1A')$ (Table 1b). The broad underlying features of this band are due to the rather antibonding σ^*_{CCl} character along the C–Cl bond (Table S5–S10), thus contributing to the background signal of the absorption spectrum.

4.3. Photon energy region 9.0 – 10.8 eV

In this energy range, the photoabsorption spectra of both TFA and CDFA arise predominantly from the contribution of members of the different Rydberg transitions converging to the $(20a')^{-1}\,\tilde{X}^2A'$ and $(8a'')^{-1}\,\tilde{A}^2A''$, and the $(32a)^{-1}\,\tilde{X}^2A$, $(31a)^{-1}\,\tilde{A}^2A$ and $(23a')^{-1}\,\tilde{X}^2A'$, $(22a')^{-1}\,\tilde{A}^2A'$ ionic states of TFA/CDFA (Section 4.4). The absorption features are also due to the overlap of the many different Rydberg electronic states and in the case of TFA to the superposition of the different vibrational quanta contributing to the absorption spectrum. These can contribute to a broadening of the absorption features, while other features appear enhanced and/or manifest themselves.

4.3.1. Trifluoroacetic acid

The electronic excitation at 9.280 eV with a cross-section of 5.17 Mb (Fig. 3a) is assigned to the Rydberg $3p'(23a')\leftarrow\bar{n}_O(20a')$, $(5^1A'\leftarrow\tilde{X}^1A')$ transition (Table 1a). The vibronic structure in this absorption band, due to the Rydberg states, is described in Section 4.4. Within the absorption band, and in the higher photon energy region, we can observe some structures (Fig. 3a) which are less abundant than in previous bands. The absorption cross-section shows two features at 9.611 and 9.999 eV and at the high end of the measured energy range 10.772 eV, with magnitudes of 9.94, 8.67 and 25.48 Mb, which have been assigned to the mixed valence-Rydberg and Rydberg transitions $\pi^*(9a'')\leftarrow\pi/n_F(6a'')+3d(26a')\leftarrow\bar{n}_O(20a')$, $(9^1A'\leftarrow\tilde{X}^1A')$, $3d(26a')\leftarrow\bar{n}_O(20a')$, $(11^1A'\leftarrow\tilde{X}^1A')$ and $3d'(27a')\leftarrow\bar{n}_O(20a')$, $(13^1A'\leftarrow\tilde{X}^1A')$ (see Table 1a). The magnitude of the cross-section increases significantly above 10 eV, where broad and weak structures above the underlying significant absorption signal are observed (Fig. 3a). In this region, the absorption spectrum is dominated by Rydberg series converging to the $(20a')^{-1}$ and the $(5a'')^{-1}$ states. The 9.0–10.8 eV band shows the contribution from the CF_3 rocking mode, $\nu'_{15}(a')$, with an average spacing of 0.044 eV (356 cm^{-1}) (see Section 4.4 and Tables 2 and S4).

4.3.2. Chlorodifluoroacetic acid

The photoabsorption energy region > 9.5 eV, shows an electronic transition peaking at 10.29(8) eV and a cross-section value of 36.07 Mb, which has been assigned to $5s(39a)\leftarrow\bar{n}_{Cl}(31a)+3d(40a)\leftarrow\bar{n}_{Cl}(30a)+3d(40a)\leftarrow n_{Cl}(31a)$, $(39^1A\leftarrow\tilde{X}^1A)/\sigma^*_{CCl}(25a')\leftarrow\sigma_{CC/CO}(21a')\ +\sigma^*_{CCl}/\pi^*(10a'')\leftarrow\bar{n}_{Cl}(6a'')$, $(19^1A'\leftarrow\tilde{X}^1A')$ for conformers #1/#2 (see Table 1b). Given the valence, mixed valence-Rydberg and Rydberg nature of the transition, the absorption band shows a relevant background signal due to σ^*_{CCl} antibonding contribution to shift the spectrum from the baseline. In this region the spectrum is also dominated by the Rydberg series converging to the $(32a)^{-1}\,\tilde{X}^2A$, $(31a)^{-1}\,\tilde{A}^2A$ and $(23a')^{-1}\,\tilde{X}^2A'$, $(22a')^{-1}\,\tilde{A}^2A'$ ionic states of CDFA acid conformer #1 and conformer #2, respectively. The Rydberg character of the electronic transitions is discussed in Section 4.4.

4.4. Rydberg series

The VUV photoabsorption spectra of TFA and CDFA above 8.2 eV show Rydberg features (Figs. 2 and 3), with the experimental energies, tentative assignments and quantum defects being given in Table 3. The calculated vertical ionisation energies at the EOM-CCSD/aug-cc-pVTZ level of theory, for TFA and CDFA are shown in Table S11. The geometries of TFA and CDFA conformers #1/#2 were kept at C_S and C_1/C_S symmetries, in the optimized ground state geometries, as indicated in Figs. S1 and S2. As far as TFA lowest-lying ionic states are concerned, we note a good agreement to within 0.1–0.2 eV with the experimental data available in the literature [12,13].

In order to tentatively assign each absorption feature position in the TFA and CDFA spectra, we have used the Rydberg formula: $E_n = IE - \frac{R}{(n-\delta)^2}$, where IE is the ionisation energy, n is the principal quantum number of the Rydberg orbital of energy E_n, R is the Rydberg constant (13.61 eV), and δ is the quantum defect resulting from the penetration of the Rydberg orbital into the core. For fluorine: $0.9<\delta<1.0$ for ns, $0.4<\delta<0.8$ for np, and $0.1<\delta<0.5$ for nd and for chlorine: $1.9<\delta<2.0$ for ns, $1.4<\delta<1.8$ for np, and $0.1<\delta<0.5$ for nd [39]. As far as the authors are aware, no previous Rydberg features of CDFA have been analysed before, hence the present assignments correspond to the most complete analysis of such states. Regarding TFA, Basch et al. [16] have reported n → 3 s and n → 3p Rydberg assignments for the absorption bands.

4.4.1. Trifluoroacetic acid

The lowest-lying Rydberg transition assigned to the $(3s\leftarrow(20a'))$ excitation, with the first member ($n=3$) at 8.44(6) eV and having a quantum defect $\delta=0.88$ (Table 3a). The quantum defect is slightly lower than the expected value for such series. A close inspection of Figs. 1a and 2a show that the shape of the absorption band is more reminiscent of a valence character rather than Rydberg. This is in assertion with the major $\pi^*(9a'')\leftarrow\pi/n_O(8a'')$ character from the calculations in Table 1a. Other transitions within the Rydberg series include the member at $n=4$ only, with $\delta=0.98$. The first members of the $(np\leftarrow20a')$ and $(np'\leftarrow20a')$ series are associated with absorption features at 9.09(0) and 9.37(9) eV ($\delta=0.60$ and 0.44, respectively) (Table 3a). Other Rydberg series members have been assigned up to 5p and 4p'. The assignments also report two nd ($nd\leftarrow20a'$) and ($nd'\leftarrow20a'$) series, with the $n=3$ features at 9.717 eV ($\delta=0.21$) and 9.919 eV ($\delta=0.03$) (Table 3a), the former appearing too intense in the absorption spectrum. This is possibly due to the mixed valence-Rydberg character of the transition and the close-lying 0^0_0 origin valence state at 9.58(2) eV (Table 2). No attempt was made to assign the higher members of the Rydberg series, due to their low intensity in the absorption spectrum or because they lie outside the energy range investigated.

The Rydberg series converging to the ionic electronic first excited state are listed in Table 3a and have been assigned to the (*ns, np* ← 8*a*″) transitions. The first members of the *ns*, and *np* series are associated with features at 9.763 eV ($\delta = 1.00$) and 10.472 eV ($\delta = 0.75$) (Table 3a). Tentative assignments of these series have only been made up to $n = 3$, because higher members lie outside the photon energy range investigated.

The vibrational progressions involving the Rydberg series converging to the $(20a')^{-1}$ and $(8a'')^{-1}$ states have been marked in Fig. 3a, with the assignments included in Table 2. The fine structure has been assigned to the CF_3 rocking, $\nu'_{15}(a')$ mode.

4.4.2. Chlorodifluoroacetic acid

The first member of the *ns* Rydberg transition for conformer #1 is assigned to (4*s* ← (32*a*)) at 8.29(9) eV and with a quantum defect $\delta = 1.97$, while $n = 5$ for the absorption feature at 10.16(3) eV and $\delta = 1.92$ (Table 3b). The feature at 8.29(9) eV can also be assigned to $4s(23a')^{-1}$. The lowest-lying members of the two n*p* (*np* ← *32a*) and (*np'* ← *21a*) series are associated with absorption features at 9.28(0) and 9.59(6) eV ($\delta = 1.58$ and 1.39) (Table 3b); these features can also be assigned to $4s(31a)^{-1}/4s(22a')^{-1}$ and $5p(23a')^{-1}$. The assignments in Table 3b also report the presence of two n*d* (*nd* ← *32a*) and (*nd;* ← *32a*) series, with their first members the $n = 3$ at 9.87(1) eV ($\delta = 0.19$) and 10.06(4) eV ($\delta = 0.02$).

Three Rydberg series converging to the ionic electronic first excited state, are listed in Table 3b and have been assigned to the (*ns, np, np'* ← 31*a*) transitions. The first members of the *ns, np* and *np'* series are associated with features at 9.28(0) eV ($\delta = 1.97$), 10.26(4) eV ($\delta = 1.58$) and 10.61(5) eV ($\delta = 1.37$). Finally, the $n = 4$p' feature at 10.61(5) eV can also be assigned to $4p'(22a')^{-1}$.

Given the expected ratio of conformer #1 to conformer #2 is ~ 9:1, there are some weak features in the spectrum that have been assigned to conformer #2. The Rydberg series converging to the ionic electronic ground state have been assigned to the (*ns, np, np', nd, nd'* ← 23*a'*) transitions. The first members of the *ns, np, np', nd* and *nd'* series are associated with features at 8.29(9) eV ($\delta = 2.00$), 9.39(3) eV ($\delta = 1.58$), 9.76(3) eV ($\delta = 1.36$), 10.01(5) eV ($\delta = 0.18$) and 10.23(0) eV ($\delta = -0.02$) (Table 3b). Moreover, the Rydberg series converging to the ionic electronic first excited state have been assigned to the (*ns, np, np'* ← 22*a'*) transitions. The first members of the *ns, np* and *np'* series are associated with features at 9.28(0) eV ($\delta = 1.96$), 10.26(4) eV ($\delta = 1.56$) and 10.61(5) eV ($\delta = 1.35$) (Table 3b). Tentative assignments of these series have only been made up to $n = 4$, because higher members lie outside the photon energy range investigated.

4.5. Absolute photoabsorption cross-sections and atmospheric photolysis

The absolute cross-section values of the electronic transitions are listed in Table 1 for TFA and CDFA, in units of Mb. A literature survey for CDFA reveals no previous ultraviolet photoabsorption data with which to compare the present work. The TFA major electronic transitions and their cross-section values in Table 1a are compared with other available absolute VUV photoabsorption cross-sections in the wavelength ranges 250–125 nm (4.96 – 9.92 eV) [16]. From the data of Basch et al. [16] the major differences are for the vertical excitation of the $1^1A''$ state the $3\,^1A'$ yielding 30 % and 16 % lower values, 0.07 and 17.59 Mb, compared to our cross-section data, 0.10 and 20.95 Mb. Rattigan et al. [17] report also at 210 nm (5.904 eV) a cross-section value of 0.07 Mb, which is 30 % lower compared to our data.

The combination of high-resolution VUV absolute photoabsorption cross-sections and solar actinic flux measurements [40], can be used to estimate photolysis rates of TFA and CDFA in the Earth's atmosphere, from 0 km altitude up to the limit of the stratopause (50 km). Since 2002 we have used this methodology to evaluate the local lifetime of a molecular compound emitted to the atmosphere and subject to the interaction of solar ultraviolet radiation only [41]. Further details can be found from the work of Limão-Vieira and co-workers [42]. The TFA quantum yield for dissociation to create OH is taken to be 0.40 at 193 nm [23], whereas a value of 1.0 is assumed for CDFA due to lack of any information in the literature.

Computed photolysis lifetimes of <10 sunlit days were calculated at altitudes above 30 km, therefore indicating that the trifluoroacetic acid molecules will be broken up by UV absorption at those altitudes. Yet, at lower altitudes the photolysis lifetimes increases to hundreds and even thousands of days close to sea-level, thus meaning that these molecules cannot be efficiently broken up by solar radiation. The kinetics and mechanisms for $^{\bullet}$OH radical reactions with TFA under atmospheric conditions, were reported by Carr et al. [5] with a rate coefficient $k \approx (1.18 \pm 0.22) \times 10^{-13}$ cm^3 molecule^{-1} s^{-1}. Later on, Hurley an co-workers [43] revised the kinetics of such reactions having obtained $k = (9.35 \pm 2.08) \times 10^{-14}$ cm^3 molecule^{-1} s^{-1}, with an estimated atmospheric lifetime of TFA with respect to reaction with OH radicals of ~230 days. Of relevance, is the vibrationally mediated overtone-induced chemical reaction of $CF_3C(O)OH{\cdot}OH$, at $\nu_{OH} = 6$ yielding CF_2CO_2 and HF products, with a calculated rate constant between 2.5×10^{-10} s^{-1} and 3.7×10^{-9} s^{-1} [19,24]. These values are in agreement with Reynard and Donaldson's results, the former for absorption into $\nu_{OH} = 6$ and the latter for $\nu_{OH} = 5$ [18]. These reactions may correspond to a lifetime that varies from 8 up to 127 years [18]. Therefore, this type of reaction may not provide the main sink

Table 3b

Energy values (eV), quantum defects (δ) and assignments of the Rydberg series converging to $(32a)^{-1}\,\tilde{X}^2A$, $(31a)^{-1}\,\tilde{A}^2A$ and $(23a')^{-1}\,\tilde{X}^2A'$, $(22a')^{-1}\,\tilde{A}^2A'$ ionic states of chlorodifluoroacetic acid conformer #1 and conformer #2, respectively. See text for details.

conformer #1						*conformer #2*					
E_n	δ	Assignment	E_n	δ	Assignment	E_n	δ	Assignment	E_n	δ	Assignment
$(IE_1)_v = 11.60$ eV $(32a)^{-1}$			**$(IE_2)_v = 12.58$ eV** $(31a)^{-1}$			**$(IE_1)_v = 11.72$ eV** $(23a')^{-1}$			**$(IE_2)_v = 12.55$ eV** $(22a')^{-1}$		
(ns ← 32a)			*(ns ← 31a)*			*(ns ← 23a')*			*(ns ← 22a')*		
8.29(9)(b)	1.97	4s	9.28(0)(s,w)	1.97	4s	8.29(9)(b)	2.00	4s	9.28(0)(s,w)	1.96	4s
10.16(3)(s,w)	1.92	5s				10.29(8)(s,w)	1.91	5s			
(np ← 32a)			*(np ← 31a)*			*(np ← 23a')*			*(np ← 22a')*		
9.28(0)(s,w)	1.58	4p	10.26(4)(s,w)	1.58	4p	9.39(3)(s,w)	1.58	4p	10.26(4)(s,w)	1.56	4p
10.45(4)(s,w)	1.55	5p				10.56(1)(s,w)	1.57	5p			
(np' ← 32a)			*(np ← 31a)*			*(np' ← 23a')*			*(np ← 22a')*		
9.59(6)(s,w)	1.39	4p'	10.61(5)(s,w)	1.37	4p'	9.76(3)(s,w)	1.36	4p'	10.61(5)(s,w)	1.35	4p'
10.56(1)(s,w)	1.38	5p'				10.68(8)(s,w)	1.37	5p'			
(nd ← 32a)						*(nd ← 23a')*					
9.87(1)(b,w)	0.19	3d				10.01(5)(b,w)	0.18	3d			
10.65(2)(b,w)	0.21	4d				10.76(3)(s,w)	0.23	4d			
(nd' ← 32a)						*(nd' ← 23a')*					
10.06(4)(s,w)	0.02	3d'				10.23(0)(b,w)	−0.02	3d'			

(b) broad feature; (s) shoulder structure; (w) weak structure (the last decimal on the energy value is given in brackets for these less-resolved features).

mechanisms in the Earth's atmosphere, while the potential to accumulate in natural water bodies may result in the major atmospheric removal mechanisms of TFA [10,43]. Recently, Garavagno et al. [10] have reported that TFA atmospheric lifetime can be reduced to 5 to 9 days if reactions with formaldehyde oxide and acetone oxide are considered. Nonetheless, precautions must be taken when considering the chemical and physical processes involved in TFA degradation in some regions across the globe. For a thorough description see [10] and references therein.

Regarding chlorodifluoroacetic acid, the lifetimes are estimated to be <1 day at altitudes above 20 km, while at lower altitudes are of the order of a couple of days. We are not aware of any study of the gas-phase kinetics for CDFA reactions with •OH radicals, to assess the role of such processes as the main sink mechanism.

5. Conclusions

The present joint experimental and theoretical work reports new absolute photoabsorption cross-section measurements of TFA and CDFA over the 4.5 to 10.8 eV photon energy range. The electronic state spectroscopy of both molecules has been comprehensively investigated with transitions assigned to valence, mixed valence-Rydberg and Rydberg character. *Ab initio* calculations at different levels of theory on the vertical excitation energies and oscillator strengths have been performed to help interpret the experimental absorption features. This has allowed spectroscopic assignments of absorption features in both molecules including assignment of fine structure in the TFA spectrum to the CF_3 rocking, $\nu'_{15}(a')$ mode.

The photolysis lifetimes of TFA and CDFA have been calculated in the Earth's atmosphere, from sea level (0 km) up to the limit of the stratopause (50 km), indicating that solar photolysis may be expected to be a relevant sink for altitudes higher than 20 km. However, gas-phase kinetics for TFA reactions with •OH radicals have been shown to be important at lower altitudes.

Supplementary material

Supplementary material associated with this article can be found, in the online version, at XXX

CRediT authorship contribution statement

P.S. Puppi: Methodology, Software. **A. Souza Barbosa:** Methodology, Software. **N.C. Jones:** Data curation, Formal analysis, Software, Validation, Writing – review & editing. **S.V. Hoffmann:** Conceptualization, Funding acquisition, Project administration, Resources, Supervision, Validation, Writing – review & editing. **U.S. Akther:** Investigation. **N.J. Mason:** Conceptualization, Funding acquisition, Investigation, Writing – review & editing. **P. Limão-Vieira:** Conceptualization, Formal analysis, Funding acquisition, Investigation, Methodology, Supervision, Writing – original draft, Writing – review & editing.

Declaration of competing interest

The authors declare that they have no known competing financial interests or personal relationships that could have appeared to influence the work reported in this paper.

Acknowledgments

PSP and ASB acknowledge support from the Brazilian agencies Conselho Nacional de Desenvolvimento Científico e Tecnológico (CNPq) and Coordenação de Aperfeiçoamento de Pessoal de Nível Superior (CAPES). PSP and ASB also acknowledge Prof. Carlos A. M. de Carvalho for computational support at LFTC-DFis-UFPR and at LCPAD-UFPR. The authors wish to acknowledge the beam time at the ISA synchrotron, Aarhus University, Denmark. PLV acknowledges the Portuguese National Funding Agency (FCT) through CEFITEC research grant UIDB/00068/2020. This work was also supported by Radiation Biology and Biophysics Doctoral Training Programme (RaBBiT, PD/00193/2012) and UCIBIO (UIDB/04378/2020). PLV also acknowledges his visiting professor position at Federal University of Paraná, Curitiba, Brazil and CAPES PrInt/UFPR.

Supplementary materials

Supplementary material associated with this article can be found, in the online version, at doi:10.1016/j.jqsrt.2024.109257.

Data availability

Data will be made available on request.

References

[1] Limão-Vieira P, Giuliani A, Delwiche J, Parafita R, Mota R, Duflot D, et al. Acetic acid electronic state spectroscopy by high-resolution vacuum ultraviolet photoabsorption, electron impact, He(I) photoelectron spectroscopy and ab initio calculations. Chem Phys 2006;324:339–49.
[2] Tang X, Madronich S, Wallington T, Calamari D. Changes in tropospheric composition and air quality. J Photochem Photobiol B 1998;46:83–95. https://doi.org/10.1016/S1011-1344(98)00187-0.
[3] Holland R, Khan MAH, Driscoll I, Chhantyal-Pun R, Derwent RG, Taatjes CA, et al. Investigation of the production of trifluoroacetic acid from two halocarbons, HFC-134a and HFO-1234yf and its fates using a global three-dimensional chemical transport model. ACS Earth Sp Chem 2021;5:849–57. https://doi.org/10.1021/acsearthspacechem.0c00355.
[4] Frank H, Klein A, Renschen D. Environmental trifluoroacetate. Nature 1996;382:34. https://doi.org/10.1038/382034a0.
[5] Carr S, Treacy JJ, Sidebottom HW, Connell RK, Canosa-Mas CE, Wayne RP, et al. Kinetics and mechanisms for the reaction of hydroxyl radicals with trifluoroacetic acid under atmospheric conditions. Chem Phys Lett 1994;227:39–44. https://doi.org/10.1016/0009-2614(94)00802-7.
[6] Martin JW, Franklin J, Hanson ML, Solomon KR, Mabury SA, Ellis DA, et al. Detection of chlorodifluoroacetic acid in precipitation: a possible product of fluorocarbon degradation. Environ Sci Technol 2000;34:274–81. https://doi.org/10.1021/es990935j.
[7] Martin JW, Mabury SA, Wong CS, Noventa F, Solomon KR, Alaee M, et al. Airborne haloacetic acids. Environ Sci Technol 2003;37:2889–97. https://doi.org/10.1021/es026345u.
[8] Lozano AI, Maioli LS, Pamplona B, Romero J, Mendes M, Silva FF, et al. Selective bond breaking of halothane induced by electron transfer in potassium collisions. Phys Chem Chem Phys 2020;22:23837–46.
[9] Silva FF, Duflot D, Hoffmann SV, Jones NC, Rodrigues FN, Ferreira-Rodrigues AM, et al. Electronic state spectroscopy of halothane as studied by ab initio calculations, vacuum ultraviolet synchrotron radiation, and electron scattering methods. J Phys Chem A 2015;119:8503–11.
[10] Garavagno M, de los A, Holland R, Khan MAH, Orr-Ewing AJ, Shallcross DE. Trifluoroacetic Acid: toxicity, sources, sinks and future prospects. Sustainability 2024;16:2382. https://doi.org/10.3390/su16062382.
[11] Lu Y, Liu L, Ning A, Yang G, Liu Y, Kurtén T, et al. Atmospheric sulfuric acid-dimethylamine nucleation enhanced by trifluoroacetic acid. Geophys Res Lett 2020;47:GL085627. https://doi.org/10.1029/2019GL085627.
[12] Åsbrink L, Svensson A. 30.4 nm He(II) photoelectron spectra of organic molecules. J Electron Spectrosc Relat Phenom 1981;24:293–314.
[13] Carnovale F, Gan TH, Peel JB. Photoelectron spectroscopic studies of the monomers and dimers of acetic and trifluoracetic acids. J Electron Spectrosc Relat Phenom 1980;20:53–67. https://doi.org/10.1016/0368-2048(80)85005-5.
[14] Sweigart DA, Turner DW. Lone pair orbitals and their interactions studied by photoelectron spectroscopy. J Am Chem Soc 1972;94:5592–8.
[15] Lesniak L, Salas J, Burner J, Diedhiou M, Burgos Paci MA, Bodi A, et al. Trifluoroacetic acid and trifluoroacetic anhydride radical cations dissociate near the ionization limit. J Phys Chem A 2019;123:6313–8. https://doi.org/10.1021/acs.jpca.9b04883.
[16] Basch H, Robin MB, Kuebler NA. Electronic spectra of isoelectronic amides, acids, and acyl fluorides. J Electron Spectrosc Relat Phenom 1968;49:4996–5000. https://doi.org/10.1063/1.1669992.
[17] Rattigan OV, Wild O, Jones RL, Cox RA. Temperature-dependent absorption cross-sections of CF3COCl, CF3COF, CH3COF, CCl3CHO and CF3COOH. J Photochem Photobiol A 1993;73:1–9.
[18] Reynard LM, Donaldson DJ. Overtone-induced chemistry of trifluoroacetic acid: an experimental and theoretical study. J Phys Chem A 2002;106:8651–7. https://doi.org/10.1021/jp021084w.
[19] Vaida V, Feierabend KJ, Rontu N, Takahashi K. Sunlight-initiated photochemistry: excited vibrational states of atmospheric chromophores. Int J Photoenergy 2008:138091. https://doi.org/10.1155/2008/138091.

[20] Kwon HT, Shin SK, Kim SK, Kim HL, Park CR. Photodissociation dynamics of acetic acid and trifluoroacetic acid at 193 nm. J Phys Chem A 2001;105:6775–9. https://doi.org/10.1021/jp010787v.
[21] Mearns AM, Back RA. The photolysis of trifluoroacetic acid vapor. Can J Chem 1963;41:1197–206. https://doi.org/10.1139/v63-168.
[22] Osborne MC, Li Q, Smith IWM. Products of the ultraviolet photodissociation of trifluoroacetic acid and acrylic acid. Phys Chem Chem Phys 1999;1:1447–54. https://doi.org/10.1039/a809064e.
[23] SenGupta S, Saha A, Kumar A, Naik PD. Photodissociation of trifluoroacetic acid at 193 nm: mechanism for formation of OH radical and stable products. J Photochem Photobiol A 2018;367:365–74. https://doi.org/10.1016/j.jphotochem.2018.08.039.
[24] Young CJ, Donaldson DJ. Overtone-induced degradation of perfluorinated alcohols in the atmosphere. J Phys Chem A 2007;111:13466–71. https://doi.org/10.1021/jp075607h.
[25] Fuson N, Josien ML, Jones EA, Lawson JR. Infrared and raman spectroscopy studies of light and heavy trifluoroacetic acids. J Chem Phys 1952;20:1627–34. https://doi.org/10.1063/1.1700229.
[26] Ito F. Infrared matrix-isolation spectroscopy of trifluoroacetic acid hydrates. Chem Phys 2011;382:52–7. https://doi.org/10.1016/j.chemphys.2011.02.010.
[27] Kagarise RE. Infrared spectrum of trifluoroacetic acid vapor. J Chem Phys 1957;27:519–22. https://doi.org/10.1063/1.1743760.
[28] Redington RL, Lin KC. Infrared spectra of trifluoroacetic acid and trifluoroacetic anhydride. Spectrochim Acta, Part A 1971;27:2445–60. https://doi.org/10.1016/0584-8539(71)80143-5.
[29] Luo C, Dong W, Gu Y. Theory-guided access to efficient photodegradation of the simplest perfluorocarboxylic acid: trifluoroacetic acid. Chemosphere 2017;181:26–36. https://doi.org/10.1016/j.chemosphere.2017.03.118.
[30] Feshin VP, Zolotarev IV, Soifer GB. Structure and internal rotation of molecules in chlorodifluoroacetic acid. J Struct Chem 2004;45:315–8. https://doi.org/10.1023/B:JORY.0000048883.74949.55.
[31] Eden S, Limão-Vieira P, Hoffmann SV, Mason NJ. VUV photoabsorption in CF3X (X = Cl, Br, I) fluoro-alkanes. Chem Phys 2006;323:313–33.
[32] Barbosa AS, Silva FF, Rebelo A, Hoffmann SV, Bettega MHF, Limão-Vieira P. Valence and Rydberg excitations of 2,4- and 2,6-difluorotoluene as studied by vacuum ultraviolet synchrotron radiation and ab initio calculations. J Phys Chem A 2016;120:8998–9007.
[33] Oliveira FVS, Barbosa AS, Jones NC, Hoffmann SV, Limão-Vieira P. The electronic spectra of 2- chlorothiophene and 3-chlorothiophene in the vacuum ultraviolet photoabsorption energy region (3.9–10.8 eV). J Quant Spectrosc Radiat Transf 2023;296:108443.
[34] Barca GMJ, Bertoni C, Carrington L, Datta D, De Silva N, Deustua JE, et al. Recent developments in the general atomic and molecular electronic structure system. J Chem Phys 2020;152:154102.
[35] Barca GMJ, Bertoni C, Carrington L, Datta D, De Silva N, Deustua JE, et al. Recent developments in the general atomic and molecular electronic structure system. J Chem Phys 2020;152:154102. https://doi.org/10.1063/5.0005188.
[36] Bauernschmitt R, Ahlrichs R. Treatment of electronic excitations within the adiabatic approximation of time dependent density functional theory. Chem Phys Lett 1996;256:454–64.
[37] Casida ME. Time-dependent density-functional theory for molecules and molecular solids. J Mol Struct-Theochem 2009;914:3–18.
[38] Randi PAS, Pastega DF, Bettega MHF, Jones NC, Hoffmann SV, Eden S, et al. Electronically excited states of formic acid investigated by theoretical and experimental methods. Spectrochim Acta, Part A 2023;289:122237. https://doi.org/10.1016/j.saa.2022.122237.
[39] Robin MB. Higher excited states of polyatomic molecules, III. Academic Press; 1985.
[40] Chemical Kinetics and Photochemical Data for Use in Stratospheric Modelling, Evaluation number 12, NASA, Jet Propulsion Laboratory. JPL 1997. Publication 97-4, January 15.
[41] Duflot D, Hoffmann SV, Jones NC, Limão-Vieira P. Synchrotron Radiation UV-VUV Photoabsorption of Gas Phase Molecules. editorsPereira AS, Tavares P, Limão-Vieira P, editors. Synchrotron Radiation UV-VUV Photoabsorption of Gas Phase Molecules. Radiat. Bioanal. Spectrosc. Tech. Theor. Methods 2019:43–81.
[42] Limão-Vieira P, Eden S, Kendall PA, Mason NJ, Hoffmann SV. VUV photoabsorption cross-section for CCl2F2. Chem Phys Lett 2002;364:535–41.
[43] Hurley MD, Andersen MPS, Wallington TJ, Ellis DA, Martin JW, Mabury SA. Atmospheric chemistry of perfluorinated carboxylic acids: reaction with OH radicals and atmospheric lifetimes. J Phys Chem A 2004;108:615–20. https://doi.org/10.1021/jp036343b.